Title

Size dependence of elastic mechanical properties of nanocrystalline aluminum

Authors

Xu, Wenwu

Dávila, Lilian P

Publication Date

2017-04-01

DOI

10.1016/j.msea.2017.03.065

Peer reviewed

Strain-induced structural modifications and size-effects in silica nanowires

Chun Tang and Lilian P. Dávila

Citation: Journal of Applied Physics **118**, 094302 (2015); doi: 10.1063/1.4929875
View online: http://dx.doi.org/10.1063/1.4929875
View Table of Contents: http://scitation.aip.org/content/aip/journal/jap/118/9?ver=pdfcov
Published by the AIP Publishing

Strain-induced structural modifications and size-effects in silica nanowires

Chun Tang and Lilian P. Dávila[a)]
Materials Science and Engineering, School of Engineering, University of California Merced, 5200 N. Lake Road, Merced, California 95343, USA

(Received 3 July 2015; accepted 20 August 2015; published online 3 September 2015)

This study investigates the structural transformations and properties of silica glass nanowires under tensile loading via molecular dynamics simulations using the BKS (Beest-Kramer-Santen) interatomic potential. Surface states of the elongated nanowires were quantified using radial density distributions, while structural transformations were evaluated via ring size distribution analysis. The radial density distributions indicate that the surface states of these silica nanowires are significantly different than those of their interior. Ring size analysis shows that the ring size distributions remain mainly unchanged within the elastic region during tensile deformation, however they vary drastically beyond the onset of plastic behavior and reach plateaus when the nanowires break. The silica nanowires undergo structural changes which correlate with strain energy and ring size distribution variations. It is also found that the ring size distribution (and strain energy) variations are dependent on the diameter of the silica nanowires. Interestingly, for ultrathin nanowires (diameters < 5.0 nm), the variation of ring size distributions shows a distinct trend with respect to tensile strain, indicating that the surface states play a key role in both modifying the mechanical properties and structural characteristics. These results for ultrathin nanowires are consistent with prior theoretical and simulation predictions. The overall findings in this study provide key insights into the novel properties of nano-sized amorphous materials, and are aimed to inspire further experiments. © *2015 AIP Publishing LLC*.
[http://dx.doi.org/10.1063/1.4929875]

I. INTRODUCTION

A wide range of silica nanostructures with precise morphologies, including nanowires (NWs), nanosprings, nanorods, and many others are readily available due to advances in contemporary synthesis methods.[1–4] Of these forms, silica nanowires have a unique one-dimensional structure and properties with potential applications in nano-electromechanical systems, such as sensors and optical devices.[5–7] To facilitate the use of silica NWs in these devices, the mechanical properties and the associated phenomena which govern such nanostructures need to be well understood. Previous studies have utilized both experimental and theoretical approaches to investigate key mechanical and structural properties of amorphous silica NWs under tension and compression.[8–14] Brambilla and Payne[3] found that the ultimate strength of silica glass NWs is around 10 GPa and is not determined by their diameters. Silva and co-investigators[8] measured the Young's modulus (E) of silica glass NWs under tension using a bending technique as well as simulations, and reported that the E value of a NW depends on the nanowire diameter. Furthermore, compressive simulations by Dávila *et al.*[9] also showed that E depends on NW diameter, that for silica glass NWs smaller than 4.0 nm in diameter, unconventional superelastic properties are exhibited, and that loading direction influences the mechanical response of these amorphous nanostructures. A recent study of the behavior of amorphous silica NWs under tension further revealed that surface states significantly affect the nanowire elastic properties and fracture mode, and also that the strain rate plays a key role in the ductile to brittle transition.[10]

Technical limitations still dictate contemporary experimentation on the properties of silica glass NWs due to manipulation and testing challenges. Despite technological advances, the current state of knowledge from experimental and simulation studies[8–14] of the structure and mechanical properties of such amorphous NWs remains relatively limited, and needs to be expanded toward realizing the full potential of these nanostructures.

The unique mechanical properties of silica NWs under external loading have raised questions about the nanostructural mechanisms or phenomena, leading to such anomalous behavior in comparison to the bulk silica state. As a typical disordered material, the response of bulk silica glass to mechanical loading has been demonstrated to be different from that of crystalline polymorphs both experimentally and theoretically.[15–20] Previous simulations have correlated the elastic-to-plastic mechanical response of bulk silica glass with structural transformations determined via ring size analysis, where ring size, n, is the shortest loop formed by n Si-O bonds.[19,20] The ring size distribution of bulk silica has been shown to have an average ring size of six ($n = 6$) and the number of rings smaller and larger than this average drops off rapidly.[19,21] High pressure or deformations can modify the structure of bulk silica and broaden this distribution as reported earlier.[20,21] Most interestingly, the changes revealed by the ring size distribution are known to characterize the "medium-range order" nature of amorphous materials.[22,23] Independent experiments on compressed bulk silica glass[24,25] have shown an enhancement of Raman lines associated with

a)Author to whom correspondence should be addressed. Electronic mail: ldavila@ucmerced.edu. Tel.: +1 209 228 4707; Fax: +1 209 228 4047

the small (three- and four-membered) rings via specific vibration frequencies. Using molecular dynamics (MD) simulations, investigators successfully reproduced the anomalous equation of state (pressure-volume) of bulk silica glass obtained under compression experiments, while the key mechanism responsible for this behavior was found to be the variation in ring size distributions.[20] This distinct structural parameter allows differentiation of silica glass from other amorphous materials. More recent MD results have revealed that the differences in the ring size distributions in the bulk and silica glass NWs are likely due to differences in densities.[9] Using scanning tunneling microscopy, Lichtenstein *et al.*[26] measured the ring size distribution at the crystalline-vitreous interface of two-dimensional silica, and found that the crystalline structural order decays gradually from the boundary to the glassy region. In addition to ring size distribution variations, bulk silica glass also exhibits unique bond angle distributions, as has been previously described in related work.[10,20]

When a silica glass NW is carved out of a simulated bulk silica glass structure, the surface area-to-volume ratio dramatically increases, representing a typical structural characteristic of silica nanowires. A recent study[10] has shown that surface states significantly modify the mechanical properties of silica nanowires. However, the effect of large structural modifications on the silica NW structures by varied mechanical strains remains unexplored. To investigate such effects, systematic MD simulations were performed to study the structural characteristics of amorphous silica NWs under tension and their relationship with surface stresses and strain energies. The significance of this study is that it can provide detailed atomistic information (not easily available in experiments) and identification of phenomena related to the nanomechanical behavior of a set of NW sizes and load conditions.

II. SIMULATION AND ANALYSIS METHODS

In this study, MD simulations were performed using the Large-scale Atomic/Molecular Massively Parallel Simulator (LAMMPS) open-source code[27] and the BKS (Beest-Kramer-Santen) interatomic potential[28] to define interactions between Si and O atoms. The BKS interatomic pair-potential has been extensively used in studies of the dynamics and structural properties of silica in many forms and conditions.[8,10,29–31]

A. Bulk silica and silica nanowire model creation

A bulk silica glass model ($14.32 \times 14.32 \times 14.32\,nm^3$) containing 192 000 atoms was first prepared using a well-established melt-quench procedure,[9,10,20] then silica NWs of a fixed length and different diameters were carved out from the bulk structure. Several amorphous silica NWs (diameters $D = 3.7$–10.0 nm, length $L = 14.32$ nm), containing 10 093–73 578 atoms were created. As reported before, this method of creating NWs has previously been found[9] to produce a very small number ($<0.5\%$) of "defects" (undercoordinated atoms) on the lateral surfaces of the nanowires; thus, these were assumed to be negligible. The resultant silica NWs were subsequently relaxed for 0.25 ns at 300 K using the canonical NVT ensemble before performing MD tensile simulations, with a random number generator used to set the initial temperature based on a Gaussian distribution. The potential energy fluctuation during the relaxation was closely examined, with results rapidly approaching saturation within 0.25 ns, indicating the NWs were fully equilibrated.

B. Silica nanowire tensile simulation

Periodic boundary conditions were used in the axial direction for the silica nanowires. For the tensile simulation, a strain rate (2%/50 ps) was applied along the axial direction of the NWs. As described previously,[10] stretching of the silica glass NWs was accomplished by repeatedly scaling the model atom coordinates in the axial direction by a factor of 1.02, and then relaxing the NW model for 25–75 ps in between rescaling steps. This loading method is comparable to techniques used in the study of amorphous silica NWs,[9] metallic NWs,[32] and bulk silica glass.[20]

C. Silica nanowire: Size-effects and structural analysis

The mechanical response and structural transformations (as measured via ring size distributions) of silica glass NWs under tension were systematically investigated. The stress-strain and strain energy curves of these NWs were first analyzed for size effects, surface states were then calculated through radial density distributions, and structural changes in the glassy wires were later evaluated using normalized ring size distributions.[9,20]

In this study, several simulated nanowires under different strain levels were analyzed separately. The radial density distribution was obtained by calculating the total number of Si and O atoms per unit cross-sectional area and then plotting this value as a function of radial position r within the nanowire. The ring size distribution was calculated using the "shortest-path" criterion,[33] assuming that stable bonds are formed at distances smaller than 2.0 Å, at different strain levels. The normalized ring size distribution was later obtained (i.e., the number of rings of certain size minus its initial value at zero strain) and plotted as a function of strain as reported before[9] to track its dependence on tensile strain and to correlate it with global deformation modes. In addition, the potential energy at each strain level was recorded and normalized to the zero strain state to analyze the strain energy variation. Lastly, the correlation of the above variables with the structural modification in several silica glass NWs was subsequently analyzed.

III. RESULTS AND DISCUSSION

To study the structural changes occurring in the amorphous silica NWs as strain increases, and to correlate them with what is known about their mechanical properties and bulk silica glass, MD tensile simulations were first performed on a selected bulk glass structure containing 12 288 atoms for comparison.

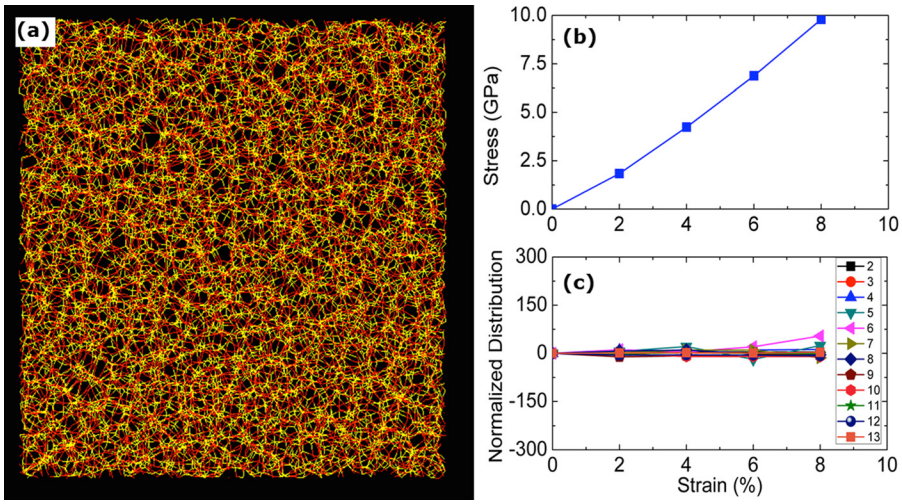

FIG. 1. A bulk silica glass structure simulated under tensile conditions at 300 K and a strain rate of 2%/50 ps shown in (a), the calculated engineering stress vs. axial engineering strain (b), and associated normalized ring size distributions (c). The number of rings of a given size ($n = 2, 3, \ldots, 12, 13$) is also shown in (c). The bulk structure shows negligible ring size variation within the elastic regime of deformation.

A. Bulk silica glass: Tensile simulation

Figure 1 shows (a) the stretched bulk silica amorphous structure, (b) calculated tensile stress-strain behavior, and (c) associated normalized ring size distributions within the elastic deformation region, confirming its non-crystalline structure is essentially unchanged. The ring size distributions for the bulk silica glass in this study (Fig. 1(c)) do not significantly change up to the highest tensile strain calculated, consistent with the linear region in its corresponding stress-strain curve (Fig. 1(b)). Thus, the resultant behavior of bulk silica glass is elastic up to 8% of strain level evaluated. This is in good agreement with previous findings for this amorphous material.[9,15–18,20]

B. Silica glass nanowires: Surface effects

When a silica NW is carved out of the bulk silica glass, the surface-to-volume ratio significantly increases, thus the surface structure will likely be different from its inner core structure and bulk counterpart, as reported recently.[10] Figure 2(a) illustrates how the radial density distribution was calculated in a NW. Figure 2(b) depicts the density distribution profile along the radial direction for a silica NW with diameter $D = 8.0$ nm, where the densities of Si and O at each radial distance r are calculated as the number of atoms per area (i.e., $2\pi r\Delta r$). A close examination of the radial density profile within the inner part of the silica NW reveals that it is relatively homogeneous; however when the radial position

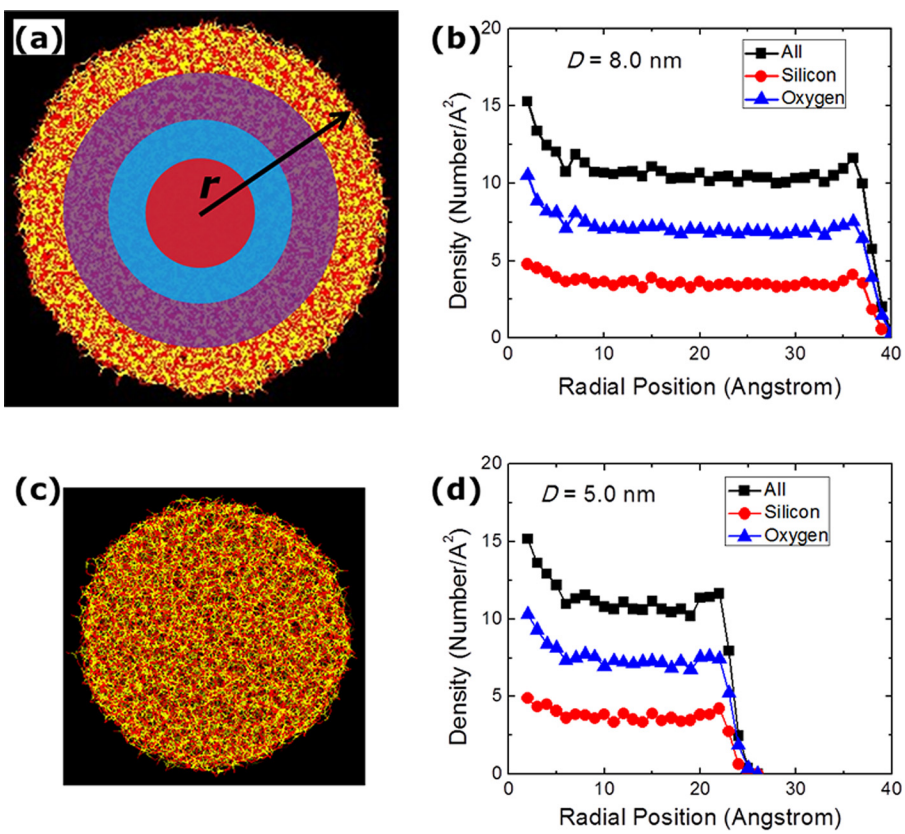

FIG. 2. Radial density distributions of two representative silica nanowires. Figure (a) illustrates how the radial density is calculated for a NW with diameter $D = 8.0$ nm (the radial position starts from the center of the nanowire outwards toward the surface, as shown by the arrow, at increasing distance r). The corresponding radial distribution is shown in (b). Figures (c) and (d) display similar results for another silica NW with smaller $D = 5.0$ nm and corresponding radial density distribution.

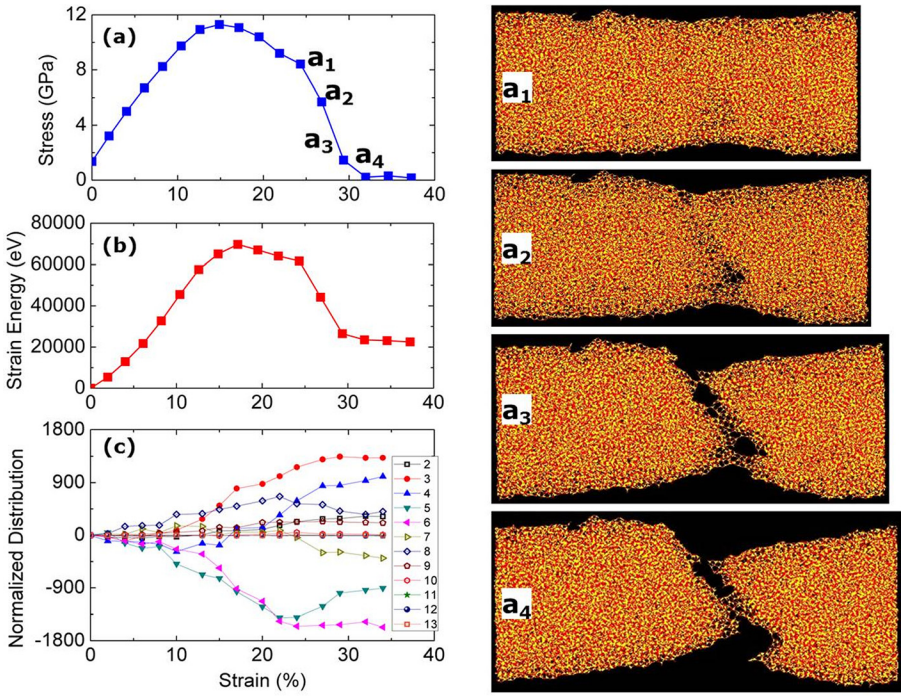

FIG. 3. MD calculated mechanical behavior of a silica glass NW ($L = 14.32$ nm, $D = 8.0$ nm) at varied tensile strains at 300 K. Results show (a) plot of the stress-strain relationship and representative snapshots revealing the structural evolution during the breaking process (from a_1 to a_4), (b) strain energy variation with respect to tensile strain, and (c) normalized ring size distributions as a function of tensile strain. The strain rate is 2%/50 ps.

approaches the surface at about 3.7 nm, the density distribution sharply decreases toward zero. The same trend can also be observed in both density profiles for Si and O atoms for this NW size and for another NW with diameter $D = 5.0$ nm (Figs. 2(c) and 2(d)). This evidence further demonstrates that the surface states of silica NWs are significantly different than those of the interior. Prior calculations of the bond angle distribution in silica NWs under tension have indicated that the reconstruction of surface bonds leads to compressed surface stress states, which modifies the NW mechanical properties when diameters are small.[10] The radial density distributions for various silica NWs resemble those shown in Figure 2.

It has been predicted by Shankar and King[34] that silica NWs would exhibit compressive surface stress states. Recent MD simulations confirmed this prediction through the observation of varying Young's modulus with decreasing NW diameter, particularly when the diameter is smaller than 4.0 nm.[10] Furthermore, in that study, it was shown that both Si-O-Si and O-Si-O bond angle distributions revealed a distinct secondary peak below the main bond angle distribution peak.[10] The secondary peak arises primarily from the surface layer of the NWs and is absent in bulk silica samples. These compacted bond angle distributions further demonstrated the compressive surface state of silica glass nanowires.

C. Silica glass nanowires: Tensile simulation and structural analysis

The effects of large strain-induced modifications on the structure of silica NWs are analyzed next using normalized ring size distributions to quantify major structural transformations. Figures 3–6 summarize the resultant strain-induced structural transformations, strain energy, and related normalized

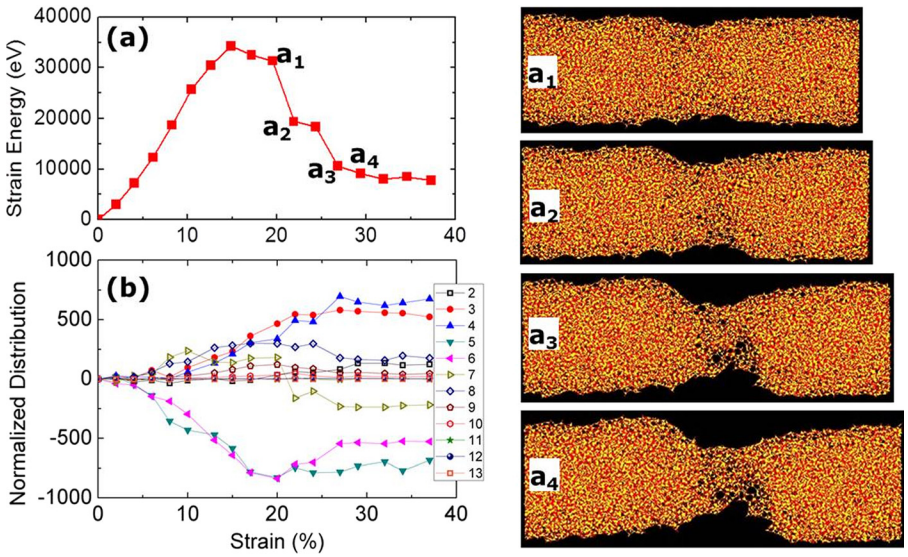

FIG. 4. MD calculated mechanical behavior of a thin silica glass NW ($L = 14.32$ nm, $D = 6.0$ nm) at varied tensile strains at 300 K. Results show (a) plot of the strain energy variation and (b) the associated normalized ring size distributions as a function of tensile strain. The strain rate remains at 2%/50 ps. Representative snapshots illustrate the structural evolution and strain levels from the stretching to the breaking stages for this amorphous wire.

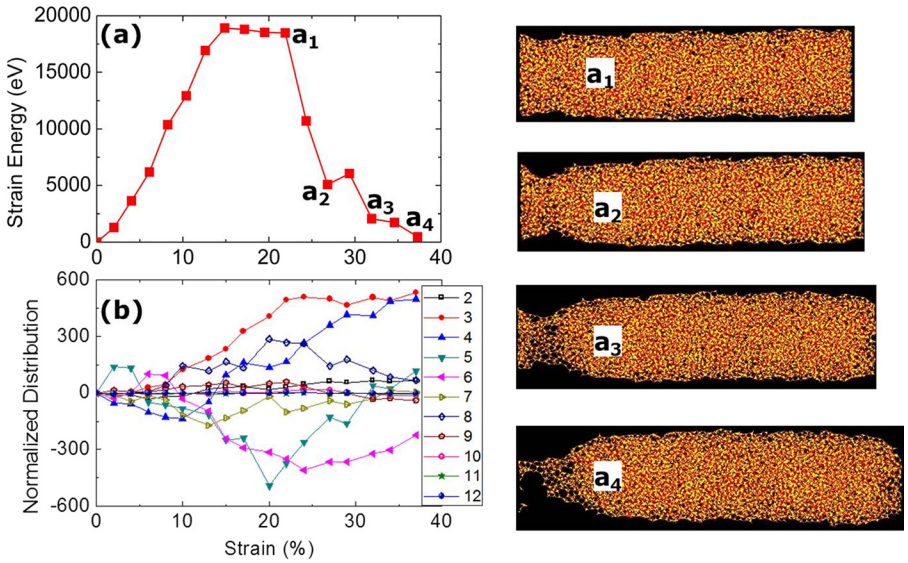

FIG. 5. MD calculated mechanical behavior of a thinner silica glass NW ($L = 14.32$ nm, $D = 5.0$ nm) at increasing tensile strains at 300 K. Results show (a) plot of the strain energy variation and (b) the associated normalized ring size distributions as a function of tensile strain. The strain rate is 2%/50 ps as in prior NW simulations. Snapshots reveal particular atomistic morphology at given strain levels during the stretching process of this NW.

ring size distributions for representative NWs as diameter decreases.

Analysis of the MD results shows how the nanostructure of silica NWs evolves as a function of tensile strain in terms of ring size distribution. As the ring size distribution is closely related to Raman spectroscopy (i.e., three- and four-membered rings are correlated with specific vibrational frequencies), therefore it can be correlated with such experimental measurements. Figure 3 illustrates representative results for a thick silica NW ($D = 8.0$ nm) under tension. The stress-strain and the strain energy-strain relationships (Figs. 3(a) and 3(b)) are plotted to possibly correlate them with the ring size distribution variations (Fig. 3(c)) as tensile strain increases. It is noteworthy that within the elastic region (less than 6% strain, as shown in Fig. 3(a)), the normalized ring size distributions (Fig. 3(c)) show minimal structural variation, consistent with our results in the bulk silica glass as shown in Fig. 1. Thus, in this region, no major structural changes are expected (i.e., no phase change, mostly bond breaking and reconstruction) in the NW during elastic deformation. Upon further stretching of the NW, it is observed that the number of five- and six-membered rings begins to decrease, as prior related findings,[9] and that of three- and eight-membered rings starts to increase, while the four-membered ring counts show an increasing trend when the tensile strain approaches ~22%. Results also indicate

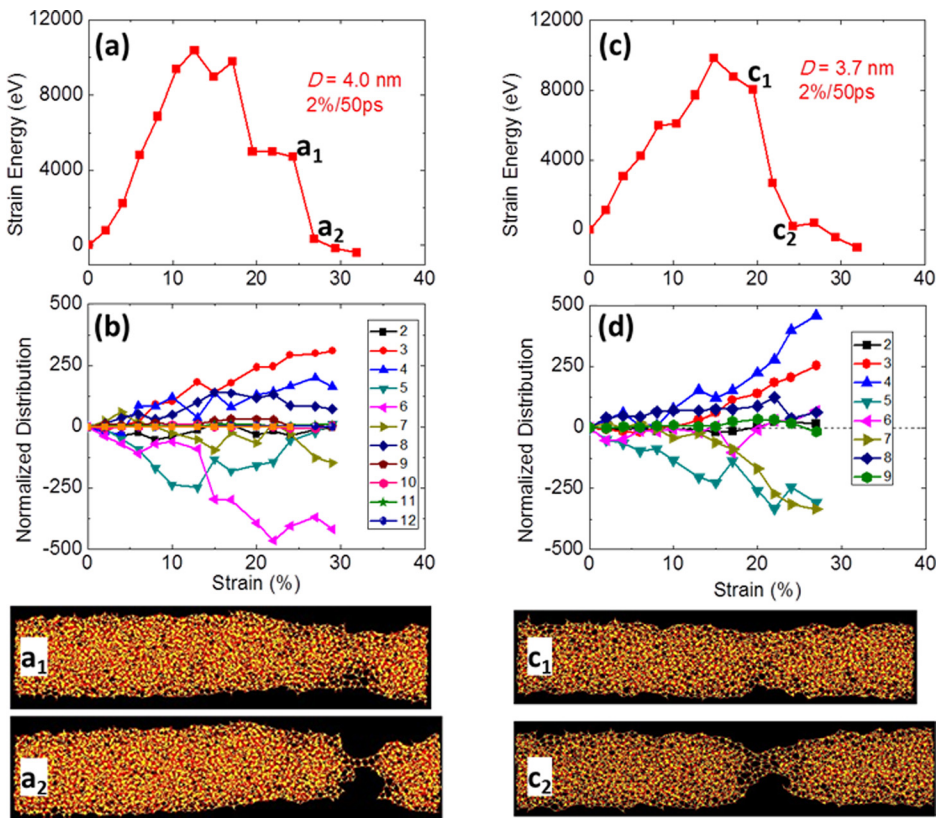

FIG. 6. MD calculated mechanical behavior of ultrathin silica glass NWs ($L = 14.32$ nm, $D = 4.0$ nm, on left, and $D = 3.7$ nm, on right) at varied tensile strains at 300 K. Results show (parts (a) and (c)) plots of the strain energy variations as strain increases and (parts (b) and (d)) the associated normalized ring size distributions as a function of tensile strain. The strain rate is 2%/50 ps. Snapshots detail evolution of morphology for these ultrathin wires.

that the plastic deformation of all NWs under tension starts at about 6% strain, although no direct structural deformation is visible during this process, with the decreasing five- and six-membered rings possibly rearranging into other ring sizes, such as the three-, four-, and eight-membered rings for energy conservation purposes. When the silica NW (Fig. 3(c) and snapshots) starts to break at ~24% strain (a_1), the number of three- and four-membered rings continues increasing, the five-membered ring count also begins to increase, the six-membered ring count reaches a plateau, and the seven- and eight-membered ring counts drop steadily, with all of these mechanisms possibly occurring to accommodate the ongoing major structural transformations in the nanowire. All other ring size distributions level off at ~24% (a_1). At this strain level, the NW undergoes major structural changes as illustrated in Fig. 3 (snapshots) which correlate well with the stress-strain, strain energy, and calculated ring size distribution variations (Figs. 3(a)–3(c)). At a higher strain of ~29% (a_3), a fracture process with no apparent plastic deformation becomes increasingly dominant (Fig. 3 snapshots), and with almost no ring structure changes. At ~32% strain (a_4), the silica NW is essentially split into two parts in the middle section, at which point all associated ring size distributions (Fig. 3(c)) level off. Hence, all simulation results indicate that this silica NW undergoes brittle behavior under tension, similar to the typical behavior observed in its bulk counterpart. This trend in fracture mode is also consistently observed in other silica glass NWs with diameters larger than 6.0 nm.

Figure 4 reveals typical tensile simulation results for a thinner silica NW ($D = 6.0$ nm) with similar trends to those observed in the thicker nanowires (Fig. 3). The stress-strain plot for this NW diameter is similar to that shown in Fig. 3(a), and previously reported elsewhere.[10] The strain energy-strain relationship (Fig. 4(a)) is plotted as function of strain for further analysis and comparison against the ring size distribution variations (Fig. 4(b)). The ring size distributions as shown in Fig. 4(b) indicate important structural variations occur between 6% and 20% (a_1) strain, where the five- and six-membered ring counts decrease more rapidly than in Fig. 3(c) and the three-, four-, and eight-membered ring counts increase steadily. This rearrangement of ring size distributions in silica can be explained as a necessary mechanism for energy conservation purposes. As strain increases (a_4) for this NW, the fracture process shows some detectable plastic deformation (Fig. 4 snapshots), with associated ring size distributions reaching similar plateaus at high strains as those observed for the thicker NW (Fig. 3).

As the silica NW diameter further decreases, different trends become obvious as shown in Figure 5 for a NW with $D = 5.0$ nm. Below a strain level of 10%, the ring size distributions (Fig. 5(b)) show slight variations, while above that level and before fracture, similar overall trends are observed as with the thicker NWs, i.e., the five- and six-membered ring counts drop in numbers (possibly by breaking into three-, four-, and eight-membered rings). However, upon stretching the silica NW to ~22% strain (a_1), although similar trends are observed as before for the three-, four-, and six-membered rings, the five-membered ring counts start to rapidly increase. As strain increases (a_4), this thinner NW begins to undergo fracture near one of its ends. Overall, the above results indicate that with decreasing silica NW diameter, the surface effects start to play a role in modifying the mechanical and structural properties of silica NWs. Prior work has predicted that when the diameter of a silica NW approaches 4.0 nm, its surface effects significantly modify the mechanical properties,[10,34] thus this result ($D = 5.0$ nm) can be considered as a transition size from larger NWs to the critical NW size of 4.0 nm and below.

Lastly, a similar analysis was pursued on silica NWs of $D = 4.0$ nm and smaller, as depicted in Figure 6. The mechanical properties and ring size distributions of two NWs were evaluated as before. Prior work showed these ultrathin NWs have distinct mechanical properties due to their abnormal surface states, as reflected by the secondary peak in the bond angle distribution.[10] In this investigation, the ring size distributions for these ultrathin silica NWs are also found to be anomalous. In particular, when the NW diameter is further reduced to 4.0 nm (Fig. 6 left), the five-membered ring distribution decreases at the early stage of stretching, but after 13% strain, it starts to increase, earlier than the equivalent strain for the $D = 5.0$ nm NW (Fig. 5), where the five-membered ring count starts to increase at ~20% strain. When the NW diameter is smaller than 4.0 nm (Fig. 6 right), it is noteworthy that the six- and seven-membered ring counts behave distinctively. The six-membered ring count remains almost unchanged even during the fracture region, while the seven-membered ring count abruptly decreases after strain level 17%, which marks the starting of plastic deformation. This can be understood from the fact that for the ultrathin NWs studied, the surface-to-volume ratio is extremely high. Thus, the typical ring size variations observed in thicker NWs contribute much less significantly to the overall behavior of these ultrathin NWs.

The above results clearly demonstrate that the ring size distribution (and strain energy) variations due to strain-induced tensile modifications are dependent on the diameter of the silica nanowires. For nanowires with a diameter larger than 5.0 nm, the three- and four-membered ring size distributions increase monotonically with tensile strain, while the five- and six-membered ring size distributions decrease. In all cases, ring size distributions reach plateaus near the strain at which the NWs break or begin to de-attach into two segments. This is consistent with the unchanging ring counts associated with highly deformed or separated NW segments. For nanowires with thinner diameters of 5.0 nm or less, the ring size distributions are more scattered, most likely due to the reduced density (i.e., number of atoms) per NW. It is also observed that as NW diameter decreases, the elastic region in the ring size distributions expands approximately from 6% to 17% strain, consistent with prior findings.[9] Although significant changes in the silica NWs are observed under tension during increasing plastic strains, the average ring size remains 6, thus the tetrahedral structure is preserved in these nanostructures.

IV. CONCLUSIONS

In summary, the structural transformation at the nanoscale of silica nanowires under tension has been investigated using atomistic simulations. MD tensile simulation results of several silica NWs at room temperature reveal that surface effects are measurable via radial density distributions. Stress-strain and strain energy calculations as a function of tensile strain correlate well with the corresponding ring size distributions for NW diameters ranging from 8.0 nm to 5.0 nm. The ring size distributions show no significant change when the silica nanowires are stretched within the elastic region but change distinctively in the plastic region. Such structural changes in silica glass NWs must be governed by the preserved connectivity (to conserve atomic bonding) of these amorphous structures, typically revealed by a decrease in five- and six-membered rings at high strains, with a corresponding increase in both smaller and larger rings as reported before.[20] After the silica nanowires are broken, the ring size distributions show no further change. Furthermore, the variation of ring counts shows a different trend versus strain when the NW diameter is smaller than 5.0 nm, consistent with the anomalous mechanical behavior and surface states reported for this critical size and below. Future studies of nanoscale structural transformations in these glassy NWs can be pursued along with spectroscopy measurements to verify these predictions; in particular, since the variation of three- and four-membered rings can be detected by Raman spectroscopy. The results of this study are expected to have key implications in the fabrication of silica nanowire-based devices, as mechanical integrity will dictate their performance.

ACKNOWLEDGMENTS

The authors thank Dr. M.-J. Caturla and Dr. J. F. Shackelford for stimulating discussions. We also want to thank Tim Allis at UC Merced for assistance in this project. This work was performed under the auspices of the NSF-funded Center of Integrated Nanomechanical Systems (COINS) award under Contract No. EEC-0832819.

[1]H. Zhang, Nano Lett. **3**, 577 (2003).
[2]Y. Qu, J. D. Carter, and T. Guo, J. Phys. Chem. B **110**, 8296 (2006).
[3]G. Brambilla and D. N. Payne, Nano Lett. **9**, 831 (2009).
[4]D. Zhang, J. Jasinski, M. Dunlap, M. Badal, V. J. Leppert, and V. Katkanant, Appl. Phys. A **92**, 595 (2008).
[5]L. Tong, J. Lou, and E. Mazur, Opt. Express **12**, 1025 (2004).
[6]L. Tong and E. Mazur, J. Non-Cryst. Solids **354**, 1240 (2008).
[7]H. Fan, C. Hartshorn, T. Buckheit, D. Tallant, R. Assink, R. Simpson, D. J. Kissel, D. J. Lacks, S. Torquato, and C. J. Brinker, Nature Mater. **6**, 418 (2007).
[8]E. C. C. M. Silva, L. Tong, S. Yip, and K. J. Van Vliet, Small **2**, 239 (2006).
[9]L. P. Dávila, V. J. Leppert, and E. M. Bringa, Scr. Mater. **60**, 843 (2009).
[10]C. Tang and L. P. Dávila, Nanotechnology **25**, 435702 (2014).
[11]Z. L. Wang, R. P. Gao, P. Poncharal, W. A. de Heer, Z. R. Dai, and Z. W. Pan, Mater. Sci. Eng., C **16**, 3 (2001).
[12]D. A. Dikin, X. Chen, W. Ding, G. Wagner, and R. S. Ruoff, J. Appl. Phys. **93**, 226 (2003).
[13]H. Ni, X. Li, and H. Gao, Appl. Phys. Lett. **88**, 043108 (2006).
[14]F. Yuan and L. Huang, Appl. Phys. Lett. **103**, 201905 (2013).
[15]H. Sugiura, R. Ikeda, K. Kondo, and T. Yamadaya, J. Appl. Phys. **81**, 1651 (1997).
[16]C. S. Zha, R. J. Hemley, H. K. Mao, T. S. Duffy, and C. Meade, Phys. Rev. B **50**, 13105 (1994).
[17]A. Polian and M. Grimsditch, Phys. Rev. B **41**, 6086 (1990).
[18]S. Susman, K. J. Volin, D. L. Price, M. Grimsditch, J. P. Rino, R. K. Kalia, P. Vashishta, G. Gwanmesia, Y. Wang, and R. C. Liebermann, Phys. Rev. B **43**, 1194 (1991).
[19]A. Kubota, M.-J. Caturla, J. S. Stolken, and M. D. Feit, Opt. Express **8**, 611 (2001).
[20]L. P. Dávila, M.-J. Caturla, A. Kubota, B. Sadigh, T. Diaz de la Rubia, J. F. Shackelford, S. H. Risbud, and S. H. Garofalini, Phys. Rev. Lett. **91**, 205501 (2003).
[21]J. F. Shackelford and R. H. Doremus, *Ceramic and Glass Materials: Structure, Properties and Processing* (Springer, New York, 2008), pp. 71–86.
[22]P. S. Salmon, Nature Mater. **1**, 87 (2002).
[23]J. D. Martin, S. J. Goettler, N. Fosse, and L. Iton, Nature **419**, 381 (2002).
[24]S. G. Demos, L. Sheehan, and M. R. Kozlowski, in Laser Applications in Microelectronics and Optoelectronic Manufacturing V: Proceedings of SPIE Int. Soc. Opt. Eng., 3933, 316 (2000); available at http://spie.org/Publications/Proceedings/Paper/10.1117/12.387569.
[25]J. W. Chan, T. R. Huser, S. H. Risbud, and D. M. Krol, Opt. Lett. **26**, 1726 (2001).
[26]L. Lichtenstein, M. Heyde, and H. Freund, Phys. Rev. Lett. **109**, 106101 (2012).
[27]S. Plimpton, J. Comput. Phys. **117**, 1 (1995).
[28]B. W. H. van Beest, G. J. Kramer, and R. A. van Santen, Phys. Rev. Lett. **64**, 1955 (1990).
[29]E. C. C. M. Silva, J. Li, D. Liao, S. Subramanian, T. Zhu, and S. Yip, J. Comput.-Aided Mater. Des. **13**, 135 (2006).
[30]K. Muralidharan, J. H. Simmons, P. A. Deymier, and K. Runge, J. Non-Cryst. Solids **351**, 1532 (2005).
[31]J. S. Tse and D. D. Klug, J. Chem. Phys. **95**, 9176 (1991).
[32]J. Diao, K. Gall, and M. L. Dunn, Nano Lett. **4**, 1863 (2004).
[33]A. B. Belonoshko, Science **275**, 955 (1997).
[34]M. R. Shankar and A. H. King, Appl. Phys. Lett. **90**, 141907 (2007).